First-principles calculation of the pressure derivative of the bulk modulus from second- and third-order elastic constants

Abhiyan Pandit[1] and Angelo Bongiorno[1,2]
[1]Department of Chemistry, College of Staten Island, Staten Island, New York 10314, USA
[2]The Graduate Center of the City University of New York, New York, New York 10016, USA

(Received 18 December 2022; revised 20 June 2023; accepted 23 June 2023; published 11 July 2023)

A first-principles method is presented to calculate the bulk modulus and its pressure derivative of a monocrystal in an arbitrary stressed state. The bulk modulus is obtained from the compliance Birch tensor, whereas its pressure derivative is calculated numerically within a nonlinear elasticity theory framework by using second- and third-order elastic constants obtained from density functional theory calculations. To demonstrate validity, generality, and accuracy, this approach is used to calculate bulk modulus and its pressure derivative of silicon and α-quartz over finite intervals of the hydrostatic pressure, and of sodium chloride at zero hydrostatic pressure and incremental differential stress. To demonstrate impact, the method is also used to elucidate the unusual elastic softening exhibited by monoclinic hafnia under hydrostatic compression.

DOI: 10.1103/PhysRevMaterials.7.073801

I. INTRODUCTION

Bulk modulus and its pressure derivative,

$$B_T = -V\left.\frac{\partial p}{\partial V}\right|_T \quad \text{and} \quad B'_T = \left.\frac{\partial B_T}{\partial p}\right|_T, \tag{1}$$

are important materials coefficients quantifying the elastic resistance to compression, and how this elastic response changes with pressure [1–6]. To determine these materials coefficients, the conventional procedure adopted in both experimental [7–14] and computational [15–20] studies consists in fitting data points of volume versus pressure with an equation of state [2–5] depending on a few free parameters, typically B_T, B'_T, and the volume of the material at zero pressure. Although straightforward and widely used, this procedure can lead to variable, and sometimes, misleading results. An example is the case of monoclinic HfO_2, a material of great technological importance [21,22]. For nearly two decades, experimental and computational studies of m-HfO_2 have used the conventional fitting procedure relying on the use of an equation of state and reported values of B_T scattered from 145 to 284 GPa [18,23,24] and from 152 to 251 GPa [15–18], respectively. In these studies, B'_T was assigned a fixed value of either 4 or 5 [16–18,23,24], a common practice adopted to reduce uncertainty of the fitting procedure. It is only very recently that high-precision x-ray diffraction experiments and a data analysis employing a Rose-Vinet equation of state [4,5] have shown that B_T has a value close to 195 GPa, and most notably that B'_T has a negative value of -5.4, indicating that m-HfO_2 exhibits the uncommon property of becoming softer upon hydrostatic compression [14]. In this work, we introduce a method, alternative to the existing one relying on a fitting procedure, to calculate reliable and accurate values of B_T, and most importantly, B'_T.

The well-established experimental approach to study materials subjected to a static pressure relies on the use of a diamond-anvil cell, combined with *in situ* characterization techniques such as x-ray diffraction, infrared, and Raman spectroscopy to monitor changes in the materials properties as a function of the pressure [7,9,12–14]. Used for a variety of purposes (including the study of solid-solid phase transitions [12], exotic electride phases in alkali metals at ultrahigh pressures [25], and the phase behavior of metallic alloys [26,27]), high-pressure experiments are used principally to probe how the volume of a material changes upon hydrostatic compression, and therefore to determine values of B_T and B'_T from fitting a set of data points of volume versus pressure [8,10,11]. Unfortunately, errors due to the challenging experimental setup, extreme pressures, purity and crystallinity of the sample, and sometimes difficult-to-control nonhydrostatic conditions often hinder the analysis of the data [18,23,24]. To reduce uncertainty of the fitting procedure, a common practice consists in assigning to B'_T a fixed value, typically around 4, and then fitting the data points with an equation of state that depends only on two free parameters: B_T and the equilibrium volume at zero pressure [9,18,23,24]. Although convenient, this solution has proven to lead to misleading results, as in the case of m-HfO_2 [14,18,23,24]. Needless to say, high-pressure experiments would greatly benefit from the availability of computational tools yielding accurate values of both B_T and B'_T.

Density functional theory (DFT) calculations are used routinely to determine values of B_T and B'_T by using the conventional approach relying on fitting values of volume versus pressure [15–20]. In these computational studies, the volume can be calculated over wide intervals of pressure, and numerical errors can be reduced to negligible values. Therefore, in principle, a fitting procedure should yield accurate values of B_T and B'_T. Unfortunately, the operation is typically carried out by fitting the data points with equations of state that, as shown in this work, can be inadequate to describe the nonlinear elastic properties of the material under compression, and thereby it can lead to unreliable results, as for example, positive instead of negative values of B'_T [15]. In this work, we devise an alternative method to calculate B_T and B'_T. In this method, DFT calculations are employed to calculate

second- and third-order elastic constants of the monocrystal in the selected stressed state. Then, the bulk modulus is calculated from the compliance Birch tensor, whereas its pressure derivative is obtained by using a numerical framework implementing equations of nonlinear elasticity theory, using the computed values of second- and third-order elastic constants as input parameters [28]. With respect to the conventional approach based on a fitting procedure, our method offers the following advantages. It is reliable, accurate, and it can be applied to any crystalline material in a given, although arbitrary, stressed state. Also, since our method requires the calculation of both second- and third-order elastic constants, it allows one to gain insight into the deformation mechanisms and nonlinear elastic terms governing the elastic response of a material under pressure.

Here, we present the conceptual background and technical aspects of our method (Sec. II), as well as its applications to silicon, α-quartz, sodium chloride, and monoclinic hafnia. In detail, in Sec. II A we introduce the relationships used to calculate the bulk modulus of a stressed monocrystal with an arbitrary symmetry from the Birch coefficients. In Sec. II B, we present our method to calculate the pressure derivative of the bulk modulus from second- and third-order elastic constants. In Sec. III, we outline the technical details of all the DFT calculations and numerical analysis carried out in this study. In Sec. IV, we present and discuss the results of our applications, and in Sec. V, we summarize the scope and main results of this work.

II. METHODOLOGY

A. Bulk modulus of a stressed monocrystal

The most common experimental approach to probe the elastic response of a material under compression is based on the use of a diamond-anvil cell [7–14]. In these experiments, the material sample is free to deform under the influence of a hydrostatic pressure, and subjected to a differential stress that typically remains small and negligible up to the ultrahigh pressure regime [11,29]. To calculate the elastic coefficient, B_T, that closely matches these experimental conditions, we use the following formula demonstrated by Wallace in Ref. [6] (the Einstein summation convention is used throughout the paper):

$$B_T = \left[\hat{B}^{(2)}_{iijj}\right]^{-1}, \tag{2}$$

where italic indices refer to Cartesian axes, and $\hat{B}^{(2)}_{ijkl}$ are the components of the tensor $\hat{\boldsymbol{B}}^{(2)}$, the tensor inverse to the Birch tensor, $\boldsymbol{B}^{(2)}$, whose components depend on the second-order elastic constants and Cauchy stress tensor of the material in the stressed reference state [6,30,31]. We underline that, as discussed in Refs. [6,30], Eq. (2) defines an elastic coefficient, B_T, quantifying how the volume of a material changes under hydrostatic compression, at constant deviatoric stress, and in the absence of rigid rotations [6,30]. Thus, among the possible different formal definitions of B_T [30], Eq. (2) is the best candidate to calculate values of B_T comparable to those obtained from measurements carried out using a diamond-anvil cell.

The components of the Birch tensor $\boldsymbol{B}^{(2)}$ are defined as follows:

$$\begin{aligned}\frac{\partial \sigma_{ij}}{\partial \varepsilon_{kl}} &= B^{(2)}_{ijkl} \\ &= C^{(2)}_{ijkl} + \frac{1}{2}\big(\sigma^{(0)}_{ik}\delta_{jl} + \sigma^{(0)}_{il}\delta_{jk} \\ &\quad + \sigma^{(0)}_{jk}\delta_{il} + \sigma^{(0)}_{jl}\delta_{ik} - 2\sigma^{(0)}_{ij}\delta_{kl}\big),\end{aligned} \tag{3}$$

where σ_{ij} and ε_{ij} are components of the Cauchy stress and infinitesimal strain tensors, respectively, and $C^{(2)}_{ijkl}$ are the second-order elastic constants of the material in a stressed state with Cauchy tensor $\sigma^{(0)}_{ij}$ [6,30,31]. It is to be noted that, although $B^{(2)}_{ijkl} \neq B^{(2)}_{klij}$ in general, the Birch coefficients $B^{(2)}_{ijkl}$ display the expected symmetries in i, j and k, l. Therefore, $\boldsymbol{B}^{(2)}$ can be written in the Voigt notation ($xx \to 1$, $yy \to 2$, $zz \to 3$, $yz \to 4$, $xz \to 5$, and $xy \to 6$) as a 6×6 matrix $b^{(2)}_{\alpha\beta}$, with $\alpha, \beta = 1 \ldots 6$, and where in general $b^{(2)}_{\alpha\beta} \neq b^{(2)}_{\beta\alpha}$; henceforth, Greek subscript indices are used to refer to tensor components in the Voigt notation, whereas italic indices are used to refer to Cartesian axes in the normal matrix convention. Thus, by defining $\hat{b}^{(2)}_{\alpha\beta}$ as the inverse matrix of $b^{(2)}_{\alpha\beta}$, Eq. (2) can be rewritten as follows:

$$\frac{1}{B_T} = K_T = \sum_{\alpha=1}^{3}\sum_{\beta=1}^{3} \hat{b}^{(2)}_{\alpha\beta}, \tag{4}$$

where K_T is the isothermal compressibility. This is the formula used in this work to calculate the bulk modulus of a monocrystalline material in an arbitrary stressed state.

It is worth noticing that in the case of a stressed material subjected to a hydrostatic pressure, i.e., $\sigma^{(0)}_{ij} = -p\delta_{ij}$, Eq. (3) can be rewritten as follows [6,31]:

$$B^{(2)}_{ijkl} = C^{(2)}_{ijkl} - p(\delta_{jl}\delta_{ik} + \delta_{il}\delta_{jk} - \delta_{ij}\delta_{kl}), \tag{5}$$

with Birch coefficients now having complete Voigt symmetry. Thus, under perfect hydrostatic conditions, Eq. (4) reduces to

$$K_T = \hat{b}^{(2)}_{11} + \hat{b}^{(2)}_{22} + \hat{b}^{(2)}_{33} + 2\big(\hat{b}^{(2)}_{12} + \hat{b}^{(2)}_{23} + \hat{b}^{(2)}_{31}\big), \tag{6}$$

which, interestingly, is identical to the Reuss's definition of B_T [32,33], commonly used to estimate, from the second-order elastic constants of the monocrystal, the isothermal compressibility and thus bulk modulus of a hypothetical polycrystalline aggregate of the same material [34]. The Reuss's definition of B_T relies on the assumption that the polycrystalline aggregate is subjected to a spatially homogeneous stress [32,33].

B. Pressure derivative of the bulk modulus

Our approach to calculate B'_T of a monocrystalline material in an arbitrary stressed state involves the following operations. First, we use the technique described in Ref. [35] to calculate both second- and third-order elastic constants of the material in the selected stressed state, that is subjected to a hydrostatic pressure p, and potentially sustaining a differential and/or shear stress. Second, we use the approach described in Ref. [28] to numerically extrapolate the second-order elastic constants of the material at hydrostatic pressures $p + \delta p$ and $p - \delta p$, calculate the corresponding bulk moduli via Eq. (4), and then obtain the desired result via numerical differentiation

as follows:

$$B'_T(p) = \frac{\partial B_T}{\partial p} \approx \frac{B_T(p+\delta p) - B_T(p-\delta p)}{2\delta p}. \quad (7)$$

For completeness, below we describe in detail the numerical operations involved in the calculation of $B_T(p \pm \delta p)$.

Let us denote with $C^{(2)}_{\alpha\beta}(p)$ and $C^{(3)}_{\alpha\beta\gamma}(p)$ the second- and third-order elastic constants of the stressed monocrystal subjected to a hydrostatic pressure p, and with Cauchy stress tensor σ^0_{ij}. In this stressed state, the geometry of the unit cell of the crystalline material is specified by the following 3×3 matrix:

$$\boldsymbol{V}(p) = \begin{pmatrix} a_{1,x} & a_{2,x} & a_{3,x} \\ a_{1,y} & a_{2,y} & a_{3,y} \\ a_{1,z} & a_{2,z} & a_{3,z} \end{pmatrix}, \quad (8)$$

where $\vec{a}_1, \vec{a}_2$, and $\vec{a}_3$ are unit cell vectors. Within a nonlinear elasticity theory treatment of the material, second- and third-order elastic constants of the material at p and with geometry $\boldsymbol{V}(p)$ can be used to estimate the Cauchy stress tensor of the same material in a deformed state. This can be accomplished by combining the following elementary relationships. First, the series expansion of the second Piola-Kirchhoff (PK2) stress tensor, P_α, truncated to the second order in the Lagrangian strain, μ_α:

$$P_\alpha(\boldsymbol{\mu}) = \sigma^0_\alpha + C^{(2)}_{\alpha\beta}(p)\mu_\beta + \tfrac{1}{2}C^{(3)}_{\alpha\beta\gamma}(p)\mu_\beta\mu_\gamma. \quad (9)$$

Second, the formulas relating PK2 stress tensor ($\boldsymbol{P}$), Lagrangian strain tensor ($\boldsymbol{\mu}$), and Cauchy stress tensor ($\boldsymbol{\sigma}$):

$$\boldsymbol{\mu} = \frac{1}{2}(\boldsymbol{F}^T\boldsymbol{F} - \mathbf{I}),$$
$$\boldsymbol{\sigma} = \frac{1}{\det \boldsymbol{F}}\boldsymbol{F}\boldsymbol{P}\boldsymbol{F}^T, \quad (10)$$

where F_α is the deformation gradient [28,35]. Thus, Eqs. (9) and (10) allow one to establish the relationship between Cauchy stress, $\boldsymbol{\sigma}$, and strain, $\boldsymbol{\mu}$, and therefore they can be used to calculate the bulk modulus of the material in a deformed state resulting from incrementing or decrementing the hydrostatic pressure by δp. This operation involves two steps.

(1) We first use Eqs. (9) and (10) to determine the geometry of the unit cell, $\boldsymbol{V}(p \pm \delta p)$, of the deformed material subjected to a hydrostatic pressure $p \pm \delta p$. To this end, we use standard numerical techniques [28] to solve Eq. (9) and find the Lagrangian strain, $\boldsymbol{\mu}$, to be applied to the reference state with geometry $\boldsymbol{V}(p)$ to increase/decrease the hydrostatic pressure by δp. We highlight that this operation is carried out by imposing that only the hydrostatic pressure p varies by $\pm\delta p$, and that deviatoric or shear stress, if present, remain constant.

(2) After having determined the deformed geometries, we use Eqs. (9) and (10) and the conventional finite deformation approach [35] to calculate the second-order elastic constants of the material at $p \pm \delta p$. This last operation requires the calculation of the PK2 stress tensor for a list of strained configurations of the material with geometries $\boldsymbol{V}(p \pm \delta p)$, and the use of first-order central finite difference formulas to calculate the elastic constants, and the corresponding $B_T(p \pm \delta p)$ via Eq. (4) [28,35]. In particular, for each strained configuration of, for example, $\boldsymbol{V}(p + \delta p)$, the PK2 stress tensor is derived by combining Eqs. (9) and (10) as outlined in the following diagram:

$$\boldsymbol{V}(p+\delta p) \xrightarrow{\tilde{\boldsymbol{\mu}}} \tilde{\boldsymbol{F}}, \tilde{\boldsymbol{V}} \xrightarrow{V(p)} \boldsymbol{\mu}, \boldsymbol{F} \xrightarrow{\boldsymbol{\mu}}$$
$$\cdots \xrightarrow{\boldsymbol{\mu}} \boldsymbol{P}(\boldsymbol{\mu}) \xrightarrow{\boldsymbol{F}} \boldsymbol{\sigma}(\boldsymbol{\mu}) = \tilde{\boldsymbol{\sigma}}(\tilde{\boldsymbol{\mu}}) \xrightarrow{\tilde{\boldsymbol{F}}} \tilde{\boldsymbol{P}}(\tilde{\boldsymbol{\mu}}), \quad (11)$$

where $\tilde{\boldsymbol{\mu}}$ and $\tilde{\boldsymbol{F}}$ are the Lagrangian strain and corresponding deformation gradient mapping $\boldsymbol{V}(p + \delta p)$ to its deformed state, $\tilde{\boldsymbol{V}}$, whereas $\boldsymbol{\mu}$ and $\boldsymbol{F}$ are the strain and deformation gradient mapping $\boldsymbol{V}(p)$ to $\tilde{\boldsymbol{V}}$. Thanks to this last correspondence, Eq. (9) can be used to extrapolate the value of the PK2 stress tensor in $\tilde{\boldsymbol{V}}$ resulting from the deformation of $\boldsymbol{V}(p)$, whereas Eq. (10) can be used to, first, calculate the Cauchy stress, $\boldsymbol{\sigma}(\boldsymbol{\mu}) = \tilde{\boldsymbol{\sigma}}(\tilde{\boldsymbol{\mu}})$, and then the PK2 stress tensor resulting from the deformation of $\boldsymbol{V}(p + \delta p)$, which is needed to calculate a second-order elastic constants [35].

We remark that in this study, we use values of δp ranging from 0.001 to 0.01 GPa. These small pressure changes lead to deformed states of a material whose unit cells $\boldsymbol{V}(p \pm \delta p)$ lie within $\leqslant 0.1\%$ in strain from the reference configuration, $\boldsymbol{V}(p)$. Also, to calculate the second-order elastic constants by using the finite deformation approach [35] and Eqs. (9) and (10), we use strain parameters as small as 10^{-4}. Since both deformed states at pressures $p \pm \delta p$ and strained configurations of $\boldsymbol{V}(p \pm \delta p)$ lie within $\sim 0.1\%$ in strain from the reference state at p, the truncated series in Eq. (9), and hence overall our method, are expected to yield accurate predictions of $P_\alpha(\boldsymbol{\mu})$ and hence B'_T [28].

III. CALCULATIONS AND DATA ANALISIS

A. DFT calculations

To carry out DFT calculations, we use the *pw.x* code of the QUANTUM ESPRESSO software package [36,37]. In particular, we consider the following materials: silicon, α-quartz, the rocksalt phase of NaCl, and the monoclinic phase of hafnia. All DFT calculations are carried out by employing primitive unit cells, ultrasoft pseudopotentials [38], and the following strict convergence criteria: 10^{-13} Ry for self-consistency, 10^{-6} a.u. for forces, and 10^{-5} kbar for the pressure.

To describe the fcc structure of silicon, we use a local density approximation functional [39], the pseudopotential *Si.pz-nl-rrkjus_psl.1.0.0.UPF* [38], a uniform mesh of $10 \times 10 \times 10\,\boldsymbol{k}$ points to sample the Brillouin zone, and plane-wave energy cutoffs of 80 and 400 Ry to represent wave functions and electron charge density, respectively. As for α-SiO_2, NaCl, and m-HfO_2, we use a generalized gradient approximation functional [40], and the following remaining technical specifications regarding types of pseudopotentials, size of the uniform mesh sampling the Brillouin zone, and plane-wave energy cutoffs to represent wave functions and electron charge density. α-SiO_2 (space group $P3_221$): *Si.pbesol-nl-rrkjus_psl.1.0.0.UPF* and *O.pbesol-nl-rrkjus_psl.1.0.0.UPF* [38], $6 \times 6 \times 6\,\boldsymbol{k}$ points, and 100 and 400 Ry. Rocksalt phase of NaCl: *Na.pbesol-spnl-rrkjus_psl.1.0.0.UPF* and *Cl.pbesol-nl-rrkjus_psl.1.0.0.UPF*, $6 \times 6 \times 6$, and 100 and 400 Ry. Monoclinic baddeleyite structure of HfO_2 (space group $P2_1/c$): *Hf.pbesol-spn-rrkjus_psl.1.0.0.UPF* and *O.pbesol-nl-rrkjus_psl.1.0.0.UPF* [38], $8 \times 8 \times 8$, and 80 and 400 Ry.

With the above technical specifications, we obtain the following lattice parameters at zero temperature and zero pressure: Si, $a = 5.400$ Å; α-SiO_2, $a = 4.972$ Å and $c = 5.462$ Å; m-HfO_2, $a = 5.045$ Å, $b = 5.114$ Å, $c = 5.217$ Å, and $\beta = 99.81^\circ$; and NaCl $a = 5.603$ Å. These parameters are in good agreement with experimental data at room temperature and ambient pressure: Si, $a = 5.431$ Å [41]; α-SiO_2, $a = 4.913$ Å and $c = 5.404\,82$ Å [42]; m-HfO_2, $a = 5.1156$ Å, $b = 5.1722$ Å, $c = 5.2948$ Å, $\beta = 99.11^\circ$ [14]; and NaCl, $a = 5.64$ Å [7].

To calculate second- and third-order elastic constants via DFT, we use the approach based on finite deformations and the numerical differentiation of the PK2 stress tensor described in Refs. [35,43]. For each material, the strained configurations are generated by using a strain parameter equal to 0.01 [35].

B. Conventional method to calculate B_T and B'_T

In the following sections, we present results obtained by using both the conventional approach and our method. For the sake of completeness, below we provide details about the conventional approach we used to calculate the values of B_T and B'_T. First, we use variable-cell DFT calculations [36,37,44] to generate a set data points of volume and pressure, $V(p)$. Second, we use an equation of state to fit the data points and determine the values of B_T and B'_T across the whole interval of pressures spanned by the calculations. In particular, we use two popular equations of state to carry out this last operation: the third-order Birch-Murnaghan [2,3] and the Rose-Vinet [4,5] equations of state. These two equations of state have the following expressions:

$$p(x) = p_0 + \frac{3}{2}B_T(x^{7/3} - x^{5/3})\left[1 + \frac{3}{4}(B'_T - 4)(x^{2/3} - 1)\right],$$

$$p(\mu) = p_0 + 3B_T\left(\frac{1-\mu}{\mu^2}\right)\exp\left[\frac{3}{2}(B'_T - 1)(1-\mu)\right], \quad (12)$$

where $x = V_0/V$ and $\mu = (V/V_0)^{1/3}$, and where V_0 is the volume at a fixed reference pressure p_0. Typically this latter parameter is set to zero. In this work, p_0 is varied across the interval of pressures spanned by the DFT calculations, and for each value we carry out the fitting operation to determine the values of V_0, $B_T(p_0)$, and $B'_T(p_0)$.

To show the limitations of the conventional approach based on the use of an equation of state, we also use higher degree polynomial functions, of degree 7 or larger, to fit the calculated $V(p)$ data points, and thus derive numerically the functions $B_T(p)$ and $B'_T(p)$. With respect to the equations of state above, which have a fixed form and depend on only three free parameters, a higher degree polynomial function depends on a larger number of free parameters, and therefore it is expected to yield unbiased and more accurate results. The results obtained by using polynomial functions are used to demonstrate both validity and accuracy of our method to calculate B_T and B'_T.

IV. RESULTS AND DISCUSSION

A. Silicon

To demonstrate validity, we first apply our method to silicon, a material exhibiting a regular and well-understood elastic response to pressure [41,45,46]. First, we employ the conventional approach. In particular, we carry out variable-cell DFT calculations [36,37,44] to optimize the volume of silicon at pressures between −2 and 8 GPa. Then, we use both the third-order Birch-Murnaghan [2,3] and Rose-Vinet [4,5] equations of state to fit the calculated volumes and derive values of B_T and B'_T across the entire interval of pressures. Second, for selected pressures, we calculate second- and third-order elastic constants [28,35], and we employ our method to calculate values of B_T and B'_T. The results of these calculations are shown in Fig. 1, together with recent experimental data [41]. For completeness, the values of both second- and third-order elastic constants of silicon are reported in Table I.

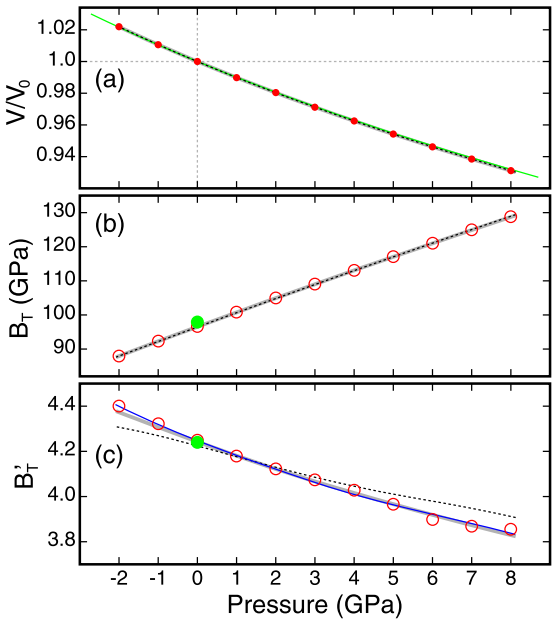

FIG. 1. (a) Relative volume, (b) bulk modulus, and (c) its pressure derivative of Si versus pressure. Red disks in (a) show results obtained from variable-cell DFT calculations. Red circles in (b) and (c) show values of $B_T(p)$ and $B'_T(p)$ obtained by using our method. Black dashed and thick gray curves show results deduced by using the third-order Birch-Murnaghan [2,3] and Rose-Vinet [4,5] equations of state, respectively. The green solid line in (a) shows the Rose-Vinet equation of state fitting the experimental data reported in Ref. [41], with $B_T = 97.89$ GPa and $B'_T = 4.24$ [green disks in (b) and (c), respectively]. The solid blue line in (c) shows the $B'_T(p)$ function derived by using a tenth-order polynomial function

The comparisons in Fig. 1 show that our method constitutes a valid alternative to the conventional approach to predict values of B_T and B'_T of a material under pressure. It is also interesting to note that the two equations of state yield different $B'_T(p)$ functions [Fig. 1(c)]. Although small in the case of Si, these differences become significant for materials such as α-quartz or m-HfO_2 (see below), and not only in the case of $B'_T(p)$ but also for $B_T(p)$. To highlight this important point, we use a higher order polynomial to interpolate the volume versus pressure data points in Fig. 1(a) and obtain the $B'_T(p)$ function from numerical differentiation. We underline again that, with respect to a typical equation of state, a higher order polynomial depends on a larger number of free parameters, and therefore it is expected to yield more accurate

TABLE I. Independent second- and third-order elastic constants Si obtained from DFT calculations [35]. Pressure and elastic constants are in GPa. For convenience, the first row shows only the Voigt indices, $\alpha\beta$ and $\alpha\beta\gamma$, of the independent $C^{(2)}_{\alpha\beta}$ and $C^{(3)}_{\alpha\beta\gamma}$, respectively.

p	11	12	44	111	112	123	144	155	456
−2.0	150	58	73	−735	−434	−76	19	−294	−55
−1.0	156	61	74	−752	−446	−82	25	−295	−52
0.0	161	64	76	−768	−459	−87	31	−295	−51
1.0	166	68	78	−785	−471	−93	37	−296	−51
2.0	172	71	79	−800	−483	−98	42	−297	−50
3.0	177	74	81	−816	−494	−103	48	−297	−50
4.0	181	77	82	−830	−506	−108	55	−297	−48
5.0	186	80	84	−846	−517	−114	60	−297	−47
6.0	191	83	85	−860	−528	−119	67	−296	−47
7.0	196	86	86	−874	−539	−124	73	−297	−45
8.0	200	89	87	−888	−549	−129	78	−297	−44

results. As shown in Fig. 1(c), and overall throughout this work, our method yields results that are in excellent agreement with those obtained by using a higher order polynomial, thus demonstrating that our method is accurate.

Our method gives a value of B'_T for silicon at zero pressure equal to 4.24, in excellent agreement with the experiment [41]. It is important to rationalize, at a semiquantitative level, the meaning of both sign and values of B'_T, and their relationships with the third-order elastic constants. To this end, we first note that under hydrostatic pressure silicon retains the fcc structure and its normal deformations can be described by a single strain parameter μ (i.e., the Lagrangian strain tensor is $\mu_{ij} = \mu\delta_{ij}$). Upon compression, changes in the second-order elastic constants, and hence bulk modulus, are controlled by the nonlinear elastic constants [6]. For example, to the first order in μ, $C^{(2)}_{11}$ varies as follows [6,47]:

$$C^{(2)}_{11}(\mu) \cong \bar{C}^{(2)}_{11} + \mu\left(\bar{C}^{(2)}_{11} + \bar{C}^{(3)}_{111} + 2\bar{C}^{(3)}_{112}\right), \qquad (13)$$

where on the right side there are the elastic constants of silicon in a reference state. As shown in Fig. 2, both $C^{(3)}_{111}$ and $C^{(3)}_{112}$ have large negative values, and since upon compression the strain parameter μ is negative, Eq. (13) clarifies and provides clues as to why $C^{(2)}_{11}$ increases monotonically across the whole interval of pressures (Fig. 2). Also, since similar arguments apply to $C^{(2)}_{12}$ (Fig. 2), B_T can only increase with pressure, thus explaining the positive sign of B'_T. It is also to be noticed that

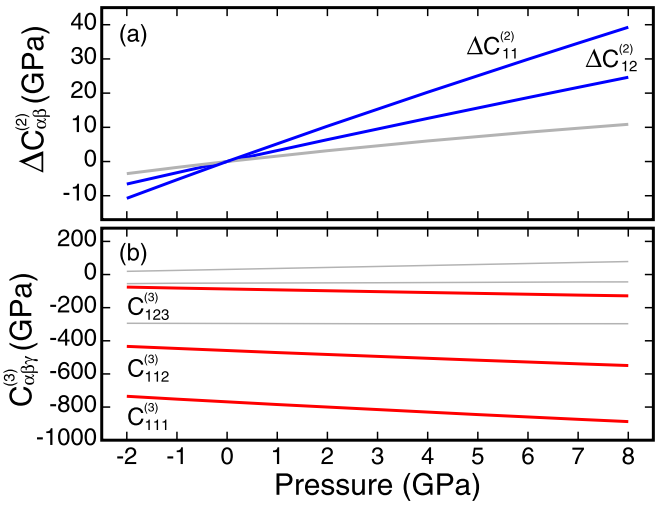

FIG. 2. Independent (a) second- and (b) third-order elastic constants of silicon versus pressure obtained from DFT calculations [35]. The values of the second-order elastic constants are referred to those at zero pressure. The red solid lines in (b) show the independent third-order elastic constants controlling the changes of $C^{(2)}_{11}$ and $C^{(2)}_{12}$ [blue lines in (a)] upon hydrostatic compression.

the third-elastic constants of silicon remain nearly constant across the entire interval of pressures (Fig. 2). This is consistent and explains the nearly constant value of B'_T across the interval of pressures, decreasing from 4.4 at −2 GPa to only about 3.8 at 8 GPa (Fig. 1).

B. α-quartz

To further demonstrate the validity and accuracy of our method, we consider the case of α-SiO_2, a crystalline material belonging to the trigonal crystal system. In particular, we calculate values of volume versus pressure, second- and third-order elastic constants (Table II), and hence values of B_T and B'_T at pressures between −2 and 8 GPa. The results of these calculations are shown in Fig. 3.

Figure 3(b) shows that the bulk moduli of α-SiO_2 calculated using Eq. (4) are in excellent agreement with the values deduced from both the equations of state and the higher degree polynomial function [for clarity, the latter function is not shown in Fig. 3(b)]. This demonstrates that Eq. (4) is sound and can be used, as an alternative to the conventional

TABLE II. Independent second- and third-order elastic constants of α-SiO_2 obtained from DFT calculations [35]. Pressure and elastic constants are in GPa. The first row shows the Voigt indices, $\alpha\beta$ and $\alpha\beta\gamma$, of independent $C^{(2)}_{\alpha\beta}$ and $C^{(3)}_{\alpha\beta\gamma}$, respectively.

p	11	12	13	14	33	44	111	112	113	114	123	124	133	134	144	155	222	333	344	444
0.0	75	1	6	19	88	52	3	−339	86	123	−277	24	−224	−26	−186	−164	−98	−623	−124	220
1.0	78	9	10	17	100	55	−175	−301	29	175	−254	−1	−278	9	−113	−92	−293	−812	−86	183
2.0	82	15	15	14	112	57	−290	−291	−13	248	−250	−16	−333	34	−123	−64	−425	−1005	−69	159
3.0	87	20	19	12	125	58	−374	−280	−31	264	−250	−32	−376	36	−109	−45	−521	−1191	−56	145
4.0	92	24	23	10	137	60	−439	−280	−45	286	−252	−35	−408	42	−107	−45	−584	−1368	−59	134
5.0	96	28	27	8	150	61	−489	−287	−55	292	−258	−47	−444	44	−111	−44	−648	−1553	−65	127
6.0	101	32	31	6	162	62	−541	−292	−59	314	−256	−49	−463	50	−111	−48	−707	−1709	−69	121
7.0	106	35	34	4	174	63	−580	−297	−57	325	−259	−50	−482	49	−112	−48	−764	−1860	−74	118

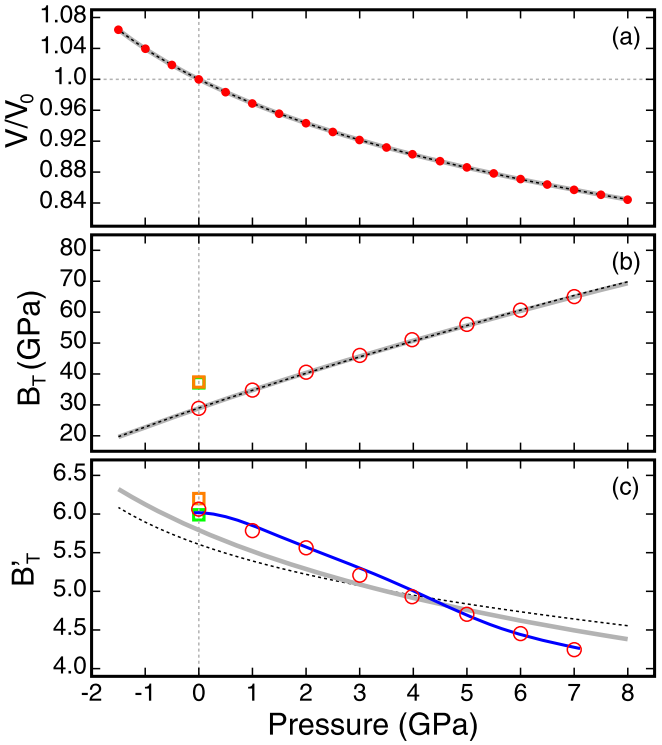

FIG. 3. (a) Relative volume (b) bulk modulus, and (c) its pressure derivative of α-SiO_2 versus pressure. Red disks show values of $V(p)$ obtained from variable-cell DFT calculations, whereas red circles show values of B_T and B'_T obtained by using our method. Black dashed and thick gray lines show results obtained by fitting the calculated $V(p)$ data points shown in (a) with a third-order Birch-Murnaghan [2,3] and Rose-Vinet [4,5] equation of state, respectively. The solid blue line in (c) shows values of B'_T obtained by interpolating the calculated $V(p)$ data points with a 10° polynomial function. Colored squares show experimental values of B_T and B'_T [42,48].

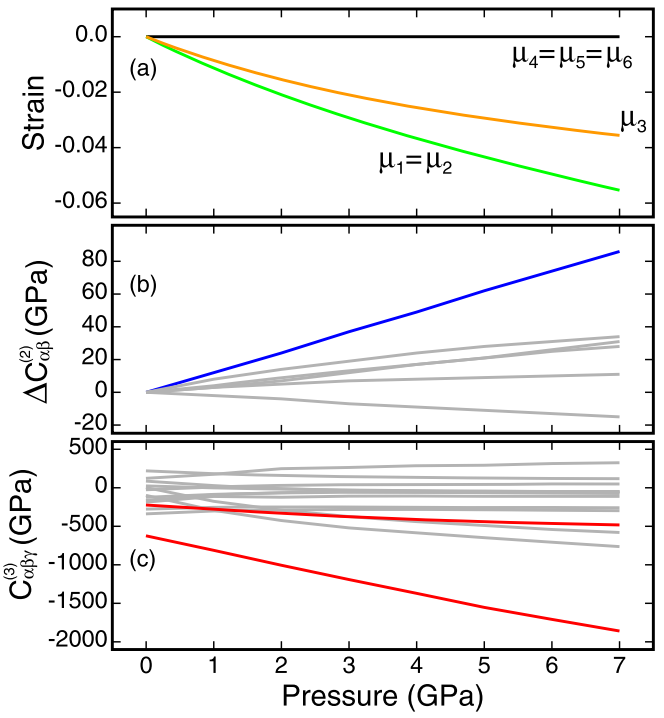

FIG. 4. (a) Lagrangian strain resulting from applying a hydrostatic pressure to α-SiO_2. (b) Independent second-order elastic constants of α-SiO_2 versus pressure referred to their values at zero pressure. The blue solid line shows values of $\Delta C^{(2)}_{33}$. (c) Independent third-order elastic constants of α-SiO_2 versus pressure. Red (gray) solid lines indicate third-order elastic constants contributing (not contributing) to the pressure-induced changes of $C^{(2)}_{33}$.

approach based on fitting $V(p)$ data points, to calculate the bulk modulus of a generic crystalline material in an arbitrary stressed state.

Figure 3(c) shows also that our results for B'_T are in excellent agreement with values derived from a high-degree polynomial function, and that a much less satisfactory agreement is reached with the results deduced from the equations of state. The third-order Birch-Murnaghan [2,3] and Rose-Vinet [4,5] equations of state have a fixed functional form with three free parameters, and it is well known that these equations can describe a restricted class of nonlinear behaviors of a $V(p)$ function [7]. In contrast, a high-degree polynomial depends on a larger number of free parameters, and it is therefore better suited to interpolate $V(p)$ functions of materials such as α-SiO_2, whose third-order elastic constants show significant variations with pressure (Fig. 4). Overall, the results in Fig. 3 further demonstrate that our method to calculate B_T and B'_T of stressed crystals is sound and accurate. We also remark that the results in Fig. 3 are in overall agreement with both experimental [42,48] and previous computational [49,50] studies of α-SiO_2.

Figure 4 shows the strain deformations occurring in α-SiO_2 upon hydrostatic compression. These results show that hydrostatic compression is accommodated by only normal strain deformations. These normal strain deformations cause all but $C^{(2)}_{14}$ to increase with pressure, thereby leading to positive values of B'_T. It is also interesting to note that the second-order elastic constant undergoing the largest increments with pressure is $C^{(2)}_{33}$. To explain this trend, we observe that, to the first order in strain, the increments with pressure of this elastic constant can be accounted for by a relationship similar to Eq. (13), which are dominated by the following two terms: $C^{(3)}_{333}\mu_3$ and $C^{(3)}_{233}\mu_2 = C^{(3)}_{133}\mu_1$. Both of these terms are the product of negative third-order elastic constants and negative strains, thereby leading to positive increments of $C^{(2)}_{33}$ with pressure (Fig. 4).

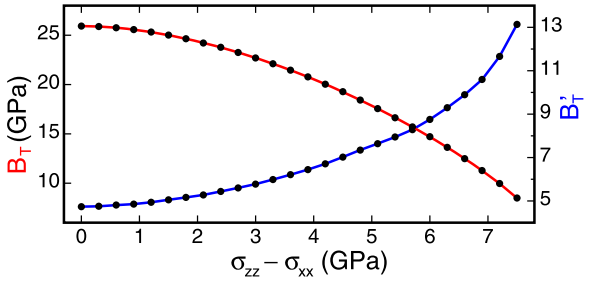

FIG. 5. Bulk modulus (red) and its pressure derivative (blue) of NaCl at zero pressure and increasing values of the differential stress, $\sigma_{zz} - \sigma_{xx} = t$, obtained by using the method presented in this work.

TABLE III. Independent second-order elastic constants of m-HfO_2 obtained from DFT calculations using the method described in Ref. [35]. Pressure and elastic constants are in GPa. The first row shows the Voigt indices of the independent $C^{(2)}_{\alpha\beta}$.

p	11	12	13	15	22	23	25	33	35	44	46	55	66
−1.0	352	178	105	47	425	169	−11	304	5	97	−10	101	143
−0.0	352	182	102	49	436	171	−12	298	9	100	−10	102	147
1.0	351	184	98	52	448	170	−11	291	13	104	−10	104	151
2.0	349	186	94	54	460	168	−10	285	19	107	−10	105	155
3.0	348	186	91	57	471	163	−8	279	24	111	−10	106	158
4.0	347	187	90	59	481	159	−6	275	29	114	−10	108	162
5.0	346	187	89	61	490	154	−4	273	33	118	−10	109	166
6.0	347	188	91	63	498	149	−1	274	37	122	−10	110	169
7.0	348	189	93	64	506	145	1	276	41	126	−9	111	172
8.0	349	191	96	65	512	142	4	280	45	129	−9	112	175
9.0	352	193	100	66	519	140	6	285	48	133	−8	113	178
10.0	354	195	104	66	526	139	8	289	51	137	−8	114	181

C. Sodium chloride

To demonstrate potential applications of our method, we consider the rocksalt phase of NaCl and we calculate B_T and B'_T of this material under different nonhydrostatic conditions, often present and difficult to control in ultrahigh-pressure experiments carried out with a diamond-anvil cell [8,10,11]. In particular, here we assume that NaCl is subjected to a zero hydrostatic pressure and shear, and with normal components

TABLE IV. Independent third-order elastic constants of m-HfO_2 obtained from DFT calculations using the method described in Ref. [35]. Pressure and elastic constants are in GPa. The first column shows the Voigt indices of the independent $C^{(3)}_{\alpha\beta\gamma}$.

p	−1.0	−0.0	1.0	2.0	3.0	4.0	5.0	6.0	7.0	8.0	9.0	10.0
111	−836	−711	−606	−550	−534	−549	−580	−616	−647	−674	−695	−714
112	−1197	−1083	−949	−829	−741	−699	−695	−718	−753	−795	−836	−880
113	277	329	327	245	104	−69	−246	−410	−545	−652	−737	−810
115	−427	−467	−494	−504	−493	−461	−425	−386	−345	−309	−274	−243
122	−1603	−1622	−1583	−1481	−1370	−1231	−1143	−1085	−1063	−1064	−1075	−1098
123	−223	−49	133	280	359	357	292	191	77	−33	−130	−218
125	101	42	−29	−94	−145	−171	−180	−175	−164	−146	−123	−111
133	584	602	538	374	125	−163	−444	−678	−850	−969	−1048	−1104
135	−646	−684	−700	−685	−640	−580	−511	−446	−392	−349	−315	−286
144	−404	−401	−397	−401	−400	−402	−406	−412	−419	−428	−438	−450
146	−8	−14	−21	−28	−36	−44	−50	−55	−58	−60	−60	−60
155	−575	−559	−544	−538	−538	−545	−554	−567	−578	−587	−598	−610
166	−1043	−1017	−1024	−1025	−1024	−1019	−1011	−1002	−991	−981	−976	−969
222	−2967	−3174	−3435	−3657	−3773	−3800	−3770	−3712	−3651	−3593	−3537	−3487
223	−2121	−2083	−1931	−1666	−1377	−1042	−795	−611	−488	−411	−357	−323
225	585	574	528	439	336	223	129	46	−20	−70	−110	−155
233	−269	63	405	700	887	947	892	770	618	471	337	227
235	24	−85	−208	−309	−389	−432	−442	−434	−414	−386	−353	−341
244	−922	−923	−923	−924	−922	−921	−920	−920	−920	−921	−923	−926
246	115	110	103	96	87	75	63	51	39	29	18	10
255	−48	−25	5	31	56	72	86	93	98	101	97	102
266	−907	−945	−966	−987	−1004	−1013	−1017	−1016	−1013	−1007	−999	−993
333	411	532	515	330	3	−412	−869	−1260	−1590	−1840	−2039	−2163
335	−1188	−1258	−1296	−1293	−1244	−1172	−1087	−1011	−949	−903	−870	−855
344	−892	−882	−868	−859	−846	−837	−829	−823	−821	−820	−821	−825
346	10	2	−9	−20	−31	−42	−50	−56	−59	−59	−59	−57
355	−458	−421	−384	−355	−333	−319	−308	−306	−299	−290	−287	−285
366	−616	−541	−530	−511	−484	−454	−422	−387	−355	−326	−304	−284
445	98	93	88	84	78	73	67	61	57	53	49	45
456	−176	−172	−167	−163	−158	−153	−147	−143	−139	−135	−132	−129
555	−253	−268	−285	−304	−321	−337	−352	−366	−379	−394	−405	−417
566	−132	−144	−148	−155	−162	−171	−182	−191	−198	−204	−209	−212

of the Cauchy stress tensor such that

$$\sigma_{xx} = \sigma_{yy} = -\frac{\sigma_{zz}}{2} = -\frac{t}{3}, \tag{14}$$

where $t = \sigma_{zz} - \sigma_{xx}$ is the uniaxial stress [8,10,11]. Thus, we employ our method to calculate B_T and B'_T of a NaCl crystal subjected to increasing values of the differential stress t.

As expected, the results of these calculations show that the occurrence of a differential stress may considerably influence the values of B_T and B'_T measured in high-pressure experiments (Fig. 5). In particular, our results agree well with experiments based on the use of a diamond-anvil cell [11], suggesting that at zero hydrostatic pressure the value of the differential stress t is smaller than 0.2 GPa, and that therefore B_T and B'_T remain close to 25.6 GPa and 5.16, respectively [11].

D. Monoclinic hafnia

To demonstrate the relevance of our method, we consider the odd case of m-HfO_2, a material whose bulk modulus softens upon compression, a behavior that still remains to be fully understood [14]. Also in this case, we first carry out DFT calculations [36,37,44] to determine the volume of m-HfO_2 for increasing values of the hydrostatic pressure (Fig. 3). Then, we use the third-order Birch-Murnaghan [2,3] and Rose-Vinet [4,5] equations of state, and higher order polynomials to fit the data points and obtain the $B_T(p)$ and $B'_T(p)$ functions in the interval of pressures ranging from 1 to 10 GPa (Fig. 3). For selected pressures, we calculate second- and third-order elastic constants [28,35] (Tables III and IV), and we use our method to calculate values of B_T and B'_T (Fig. 6). These calculations show that the equations of state not only fail to reproduce the correct behavior of $B'_T(p)$, but interestingly also of $B_T(p)$. In contrast, Fig. 6 shows that our method yields accurate predictions across the entire interval of pressures, in close agreement with results obtained by using higher order polynomial functions. Overall, these results show that our method is accurate and general.

Materials with a negative B'_T are rare [51–54], and the mechanisms responsible for this odd behavior remain unclear [55]. In particular, to the best of our knowledge, so far this property has been observed in silica [51,52], metallic glasses [53], and the isostructural monoclinic phases of zirconia and hafnia [14,54,55]. To elucidate the puzzling elastic behavior of m-HfO_2, we inspect our results, and we find that in this material, hydrostatic compression triggers deformations that are anisotropic and involve significant shearing (Fig. 7). Both lattice parameters a and c undergo contraction, b remains practically constant up to 10 GPa, and the angle between the a and c axes, β, decreases, leading to a positive shear strain μ_5 (Fig. 7). These pressure-induced deformations are accommodated in a rather peculiar way by the structure of m-HfO_2, which consists of a regular arrangement of edge-sharing distorted capped trigonal prisms, with O atoms at vertices and Hf atoms occupying central positions of the prisms (Fig. 7). In particular, upon compression each prism twists and deforms in such a way that three out of seven Hf-O bonds increase rather than decrease their length (Fig. 7). The lengthening of these Hf-O bonds suggests and is consistent with the softening of B_T upon compression exhibited by m-HfO_2.

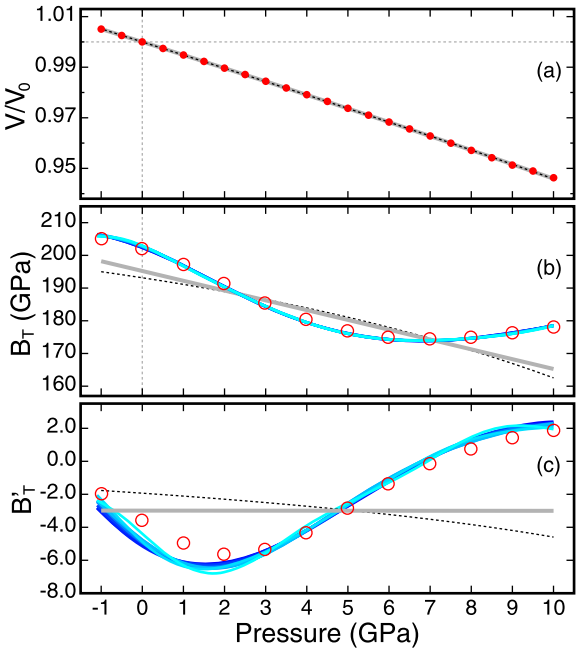

FIG. 6. (a) Relative volume, (b) bulk modulus, and (c) its pressure derivative of m-HfO_2 versus pressure. Red disks and circles show results obtained from DFT calculations. Black dashed and thick gray lines show the results of fitting the data in (a) with the third-order Birch-Murnaghan [2,3] and Rose-Vinet [4,5] equations of state, respectively. The solid cyan-blue lines show results derived by using polynomial functions of degree 7–15.

To gain a deeper understanding, we inspect the values of the second- and third-order elastic constants used to calculate the function $B'_T(p)$ (Tables III and IV and Fig. 8). These results show that upon compression, the second-order elastic constants $C_{33}^{(2)}$, $C_{23}^{(2)}$, and $C_{11}^{(2)}$ decrease, rather than increase, and that up to about 6 GPa, these constants are responsible for the negative sign of $B'_T(p)$ (Fig. 6). As discussed above

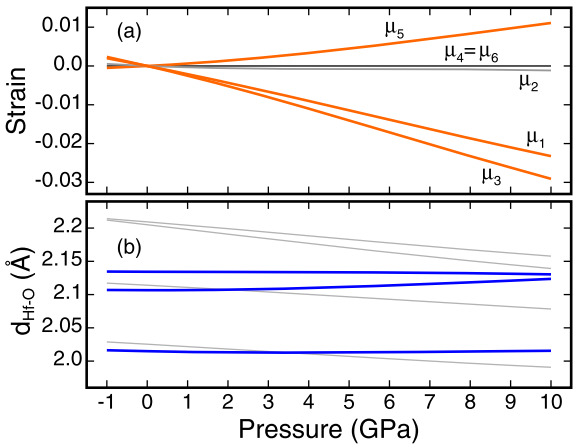

FIG. 7. (a) Strain deformations of m-HfO_2 versus hydrostatic pressure. (b) Length of the inequivalent first nearest-neighbor Hf-O bonds versus pressure. Blue and gray solid lines show bonds whose lengths increase and decrease for increasing values of p, respectively. Inset in (a) shows the prism making up the lattice of m-HfO_2.

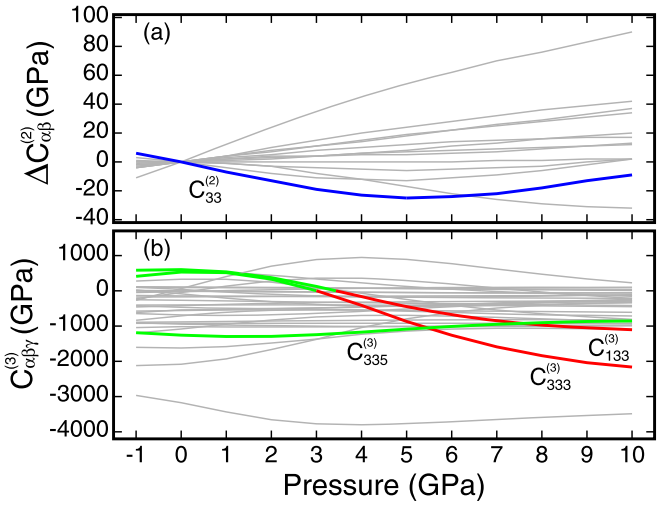

FIG. 8. (a) Second-order elastic constants, relative to their values at zero pressure, and (b) third-order elastic constants of m-HfO_2 versus pressure calculated from DFT [35]. Colored lines in (b) show the third-order elastic constants leading to increasing (green) and decreasing (red) the value of $C^{(2)}_{33}$ [blue line in (a)] for increasing the hydrostatic pressure.

for the case of both silicon and α-SiO_2, upon hydrostatic compression the variation of a second-order elastic constant, $\Delta C^{(2)}_{\alpha\beta}$, is the result of a linear combination of terms as $C^{(3)}_{\alpha\beta\gamma}\mu_\gamma$ [Eq. (13)]. For example, Fig. 8 shows that, due to the peculiar nature of the deformations occurring in m-HfO_2 upon hydrostatic compression, the value of $C^{(2)}_{33}$ is mostly affected by the terms $C^{(3)}_{335}\mu_5$, $C^{(3)}_{133}\mu_1$, and $C^{(3)}_{333}\mu_3$. $C^{(3)}_{335}$ has a nearly constant and large negative value, and because of the positive shearing deformation, the corresponding term contributes to reduce $C^{(2)}_{33}$ across the entire interval of pressures. The remaining two terms contribute to further decrement $C^{(2)}_{33}$ up to around 3 GPa, i.e., until $C^{(3)}_{133}$ and $C^{(3)}_{333}$ have a positive sign. After this point, these two last terms begin to contribute to increasing the value of $C^{(2)}_{33}$. These trends explain the behavior of B'_T with pressure shown in Fig. 6, decreasing to a value of about −6 at around 2–3 GPa, and then increasing and reaching a zero value at about 6 GPa. Overall, the arguments above suggest that the unusual elastic softening of m-HfO_2 arises from the occurrence of both positive shear deformations upon hydrostatic compression and strong elastic nonlinearities, as indicated by the variation with pressure in both sign and value of both $C^{(3)}_{133}$ and $C^{(3)}_{333}$ (Fig. 8).

V. CONCLUSION

We have introduced a general and reliable formalism to calculate accurate values of the bulk modulus and its pressure derivative of a monocrystal in an arbitrary stress state. This method involves the calculation of second- and third-order elastic constants by using a DFT approach [35], and the numerical solution of elementary equations of nonlinear elasticity theory [28]. Although general, this method is suited to be applied to low-symmetry materials exhibiting strong elastic nonlinear properties, i.e., materials whose third-order elastic constants are subjected to large variations upon compression, and thus materials for which the conventional approach based on the use of equations of state is likely to yield unreliable results. In the particular case of m-HfO_2, we have shown that the unusual negative value of B'_T originates from the occurrence of both shear deformations upon compression and strong elastic nonlinearities.

ACKNOWLEDGMENTS

This work is supported by the National Science Foundation (NSF), Awards No. DMR-2036176 and No. OAC-2215760. We also acknowledge the support of the CUNY High Performance Computing Center.

[1] O. L. Anderson, *Equation of State of Solids for Geophysics and Ceramic Science* (Oxford University Press, New York, 1995).
[2] F. D. Murnaghan, Proc. Natl. Acad. Sci. USA **30**, 244 (1944).
[3] F. Birch, Phys. Rev. **71**, 809 (1947).
[4] P. Vinet, J. Ferrante, J. R. Smith, and J. H. Rose, J. Phys. C: Solid State Phys. **19**, L467 (1986).
[5] P. Vinet, J. R. Smith, J. Ferrante, and J. H. Rose, Phys. Rev. B **35**, 1945 (1987).
[6] D. C. Wallace, Phys. Rev. **162**, 776 (1967).
[7] A. M. Hofmeister, Phys. Rev. B **56**, 5835 (1997).
[8] A. K. Singh, C. Balasingh, H.-k. Mao, R. J. Hemley, and J. Shu, J. Appl. Phys. **83**, 7567 (1998).
[9] O. Ohtaka, H. Fukui, T. Kunisada, T. Fujisawa, K. Funakoshi, W. Utsumi, T. Irifune, K. Kuroda, and T. Kikegawa, Phys. Rev. B **63**, 174108 (2001).
[10] H. Dong, D. He, T. S. Duffy, and Y. Zhao, Phys. Rev. B **79**, 014105 (2009).
[11] L. Xiong, L. Bai, and J. Liu, J. Appl. Phys. **115**, 033509 (2014).
[12] E. Bykova1, L. Dubrovinsky, N. Dubrovinskaia, M. Bykov, C. McCammon, S. Ovsyannikov, H.-P. Liermann, I. Kupenko, A. Chumakov, R. Rüffer *et al.*, Nat. Commun. **7**, 10661 (2016).
[13] K. F. Dziubek, M. Ende, D. Scelta, R. Bini, M. Mezouar, G. Garbarino, and R. Miletich, Nat. Commun. **9**, 3148 (2018).
[14] Y. Akahama, S. Kawaguchi, N. Hirao, and Y. Ohishi, Appl. Phys. Lett. **117**, 182903 (2020).
[15] J. E. Lowther, J. K. Dewhurst, J. M. Leger, and J. Haines, Phys. Rev. B **60**, 14485 (1999).
[16] J. Kang, E.-C. Lee, and K. J. Chang, Phys. Rev. B **68**, 054106 (2003).
[17] J. E. Jaffe, R. A. Bachorz, and M. Gutowski, Phys. Rev. B **72**, 144107 (2005).
[18] Y. Al-Khatatbeh, K. K. M. Lee, and B. Kiefer, Phys. Rev. B **82**, 144106 (2010).
[19] K. Lion, P. Pavone, and C. Draxl, Phys. Rev. Mater. **6**, 013601 (2022).
[20] Z. Zhang and R. M. Wentzcovitch, Phys. Rev. B **106**, 054103 (2022).

[21] X. Xu, F.-T. Huang, Y. Qi, S. Singh, K. M. Rabe, D. Obeysekera, J. Yang, M.-W. Chu, and S.-W. Cheong, Nat. Mater. **20**, 826 (2021).
[22] Y. Yun, P. Buragohain, M. Li, Z. Ahmadi, Y. Zhang, X. Li, H. Wang, J. Li, P. Lu, L. Tao *et al.*, Nat. Mater. **21**, 903 (2022).
[23] J. M. Leger, A. Atouf, P. E. Tomaszewski, and A. S. Pereira, Phys. Rev. B **48**, 93 (1993).
[24] S. Desgreniers and K. Lagarec, Phys. Rev. B **59**, 8467 (1999).
[25] D. N. Polsin, A. Lazicki, X. Gong, S. J. Burns, F. Coppari, L. E. Hansen, B. J. Henderson, M. F. Huff, M. I. McMahon, M. Millot *et al.*, Nat. Commun. **13**, 2534 (2022).
[26] C. L. Tracy, S. Park, D. R. Rittman, S. J. Zinkle, H. Bei, M. Lang, R. C. Ewing, and W. L. Mao, Nat. Commun. **8**, 15634 (2017).
[27] M. Frost, E. E. McBride, J. S. Smith, and S. H. Glenzer, Sci. Rep. **12**, 12341 (2022).
[28] A. Bakare and A. Bongiorno, Phys. Rev. Mater. **6**, 043803 (2022).
[29] Y. Akahama, H. Kawamura, and A. K. Singh, J. Appl. Phys. **95**, 4767 (2004).
[30] V. I. Levitas, Phys. Rev. B **104**, 214105 (2021).
[31] T. H. K. Barron and M. L. Klein, Proc. Phys. Soc. **85**, 523 (1965).
[32] A. Reuss, Z. Angew. Math. Mech. **9**, 49 (1929).
[33] R. Hill, Proc. Phys. Soc. A **65**, 349 (1952).
[34] M. de Jong, W. Chen, T. Angsten, A. Jain, R. Notestine, A. Gamst, M. Sluiter, C. K. Ande, S. van der Zwaag, J. J. Plata *et al.*, Sci. Data **2**, 150009 (2015).
[35] T. Cao, D. Cuffari, and A. Bongiorno, Phys. Rev. Lett. **121**, 216001 (2018).
[36] P. Giannozzi, S. Baroni, N. Bonini, M. Calandra, R. Car, C. Cavazzoni, D. Ceresoli, G. L. Chiarotti, M. Cococcioni, I. Dabo *et al.*, J. Phys.: Condens. Matter **21**, 395502 (2009).
[37] P. Giannozzi, O. Andreussi, T. Brumme, O. Bunau, M. B. Nardelli, M. Calandra, R. Car, C. Cavazzoni, D. Ceresoli, M. Cococcioni *et al.*, J. Phys.: Condens. Matter **29**, 465901 (2017).
[38] A. D. Corso, https://github.com/dalcorso/pslibrary.
[39] J. P. Perdew and A. Zunger, Phys. Rev. B **23**, 5048 (1981).
[40] J. P. Perdew, A. Ruzsinszky, G. I. Csonka, O. A. Vydrov, G. E. Scuseria, L. A. Constantin, X. Zhou, and K. Burke, Phys. Rev. Lett. **100**, 136406 (2008).
[41] S. Anzellini, M. T. Wharmby, F. Miozzi, A. Kleppe, D. Daisenberger, and H. Wilhelm, Sci. Rep. **9**, 15537 (2019).
[42] R. J. Angel, D. R. Allan, R. Miletich, and L. W. Finger, J. Appl. Cryst. **30**, 461 (1997).
[43] A. Pandit and A. Bongiorno, Comput. Phys. Commun. **288**, 108751 (2023).
[44] R. M. Wentzcovitch, J. L. Martins, and G. D. Price, Phys. Rev. Lett. **70**, 3947 (1993).
[45] H. J. McSkimin and P. Andreatch, J. Appl. Phys. **35**, 2161 (1964).
[46] J. Philip and M. A. Breazeale, J. Appl. Phys. **54**, 752 (1983).
[47] H. Wang and M. Li, Phys. Rev. B **85**, 104103 (2012).
[48] J. Wang, Z. Mao, F. Jiang, and T. S. Duffy, Phys. Chem. Minerals **42**, 203 (2015).
[49] H. Kimizuka, S. Ogata, J. Li, and Y. Shibutani, Phys. Rev. B **75**, 054109 (2007).
[50] M. Murri and M. Prencipe, Entropy **23**, 1366 (2021).
[51] E. H. Bogardus, J. Appl. Phys. **36**, 2504 (1965).
[52] K. Kondo, S. Iio, and A. Sawaoka, J. Appl. Phys. **52**, 2826 (1981).
[53] Q. Zeng, Z. Zeng, H. Lou, Y. Kono, B. Zhang, C. Kenney-Benson, C. Park, and W. L. Mao, Appl. Phys. Lett. **110**, 221902 (2017).
[54] M. Fujimoto, Y. Akahama, H. Fukui, N. Hirao, and Y. Ohishi, AIP Adv. **8**, 015310 (2018).
[55] H. Fukui, M. Fujimoto, Y. Akahama, A. Sano-Furukawa, and T. Hattori, Acta Crystallogr., Sect. B: Struct. Sci., Cryst. Eng. Mater. **75**, 742 (2019).